Accepted, JPO, Oct 2019

ACC SUBDUCTION BY MESOSCALES

V.M. Canuto[1, 2] and Y.Cheng[1, 3]

[1]NASA, Goddard Institute for Space Studies, 2880 Broadway, New York, NY, 10025; [2]Dept. of Applied Phys. and Math., Columbia University, New York, NY, 10027; [3]Center for Climate Systems Research, Columbia Univ., New York, NY, 10025.

Corresponding author: vmcanuto@gmail.com

Abstract

The mesoscale contribution to Subduction in the Southern Ocean was recently studied by Salle'e and Rintoul (2011, SR) using the following mesoscale model. The adiabatic A-regime was modeled with the GM stream function, the diabatic D-regime was modeled with tapering functions, the D-A interface was taken to be at the mixed layer depth and the mesoscale diffusivity was either a constant or given by a 2D model. Since the resulting subductions were an order of magnitude smaller than the data of ±200 m/yr (Mazloff et al., 2010), SR showed that if instead of the above model-dependent mesoscale diffusivities, they employed the ones by Salle'e et al. (2008) from surface drifter observations, the subductions compared significantly better with the data. On those grounds, SR suggested a tenfold increase of the diffusivity.

In this work, we suggest that since the mesoscale diffusivity is but one component of a much large mesoscale parameterization, one should first assess the latter's overall performance followed by the assessment of the predicted ACC subduction. We employ the mesoscale model formulated in Canuto et al. (2018; 2019, that includes recent theoretical and observational advances and that was assessed against a variety of data including the output of 17 other OGCMs. The ACC diffusivities compare well with drifter data by Salle'e et al. (2008) and the ACC subduction rates are in agreement with the data.

1. Salle′e-Rintoul model

Subduction irreversibly transfers water masses from the mixed layer depth H to the interior thermocline. The form of the *subduction rate* S_b reads as follows (Cushman-Roisin, 1987; Marshall, 1997):

$$S_b = \frac{\partial H}{\partial t} + \underbrace{\overline{\mathbf{u}} \cdot \nabla H + \overline{w}}_{mean} + \underbrace{\mathbf{u}^{+} \cdot \nabla H + w^{+}}_{eddy} = \frac{\partial H}{\partial t} + S_b(\text{mean}) + S_b(\text{eddy}) \tag{1.1}$$

Sloyan and Rintoul (2001), Salle′e et al. (2010) and Salle′e and Rintoul (2011, SR) computed $S_b(\text{eddy})$ and Salle′e et al. (2010, sec. 4b) concluded that the eddy component “plays an order one role in the overall subduction in the Southern Ocean”. SR employed the following model:

1. **Adiabatic-A regime**. It was treated using the GM stream function $\mathbf{\Psi}_A$ (Gent and McWilliams, 1990):

$$\mathbf{\Psi}_A = -\kappa_M \mathbf{s} \times \mathbf{e}_z \tag{1.2}$$

where κ_M is the mesoscale diffusivity, $\mathbf{s}$ ($= -N^{-2}\nabla_H \overline{b}$) is the slope of the isopycnals and $\mathbf{e}_z = (0,0,1)$,

2. **Diabatic-D regime**. It was parameterized as an extension of the A-regime using:

$$\mathbf{\Psi}_D = -\kappa_M T(x,y,z)\mathbf{s} \times \mathbf{e}_z \tag{1.3}$$

where the tapering function T(x,y,z) was assumed to depend only on z with the boundary conditions T(0)=0 and T(A-D interface) =1,

3. The A-D interface was taken at H,
4. The mesoscale diffusivity was taken to be:

$$\kappa_M = 10^3\,m^2 s^{-1} \quad \text{and} \quad \text{2D (Visbeck et al., 1997)} \tag{1.4}$$

Fig.4 of SR shows that the predicted subduction rates are an order of magnitude smaller than the data of ±200 m/yr (Mazloff et al., 2010; cited as SOSE, Southern Ocean State Estimate). On the other hand, use of the diffusivities derived by Salle'e et al. (2008) from surface drifter observations, yielded subductions that compared significantly better with the data. On those grounds, SR suggested a tenfold increase of the mesoscale diffusivity in relations (1.2)-(1.4).

Since the mesoscale diffusivity is but one component of a complete mesoscale parameterization, we suggest that fthe latter should first be assessed on its overall performance, the ACC subduction being one of the tests. We employ the mesoscale models presented in Canuto et al. (2018; 2019, C18, C19) that include recent theoretical and observational advances and that were assessed against a variety of data and the outputs of 17 other OGCMs (Griffies et al., 2009). The model yields two main results: the ACC diffusivities compare well with those from drifter data (Salle'e et al., 2008) and the ACC subduction rates are of the same magnitude of the SOSE data.

2. New mesoscale model

For the reader's convenience, we have added Appendix A with the relevant equations of C18 and C19.

a) A-regime

A census of Topex-Poseidon T/P altimetry data led Chelton et al. (2011, C11) to the conclusion that "essentially all of the observed mesoscale features are highly non-linear" which calls for a non-linear treatment of mesoscales. Six years before C11, a non-linear mesoscale model was proposed (Canuto and Dubovikov, 2005, CD5) but lack of data did not allow the assessment of the model's two key predictions: *first*, mesoscales do not travel with the mean velocity but with their own *drift velocity* $\mathbf{u}_d$ which is a barotropic variable since is the solution of an eigenvalue problem. The T/P-based conclusions by C11 confirmed the prediction and defined $\mathbf{u}_d$ as the most germane of all the nonlinear metrics. It must be noted that $\mathbf{u}_d$ cannot be identified with the Rossby phase velocity resulting from linear analysis and which does not reproduce altimetry data (Klocker and Marshall, 2014). Fig.1 of Canuto et al. (2018, C18) shows that the form of $\mathbf{u}_d$ given by Eq.(2.5) of C18 compares well with altimetry data. *Second,* the eddy-induced velocity is no longer given by the GM form alone since $\mathbf{u}_d$ introduces a second term:

$$\mathbf{u}^{+}=-\frac{\partial}{\partial z}\kappa_M\mathbf{s} \quad - \quad \frac{\kappa_M}{\sigma f r_d^2}\mathbf{e}_z\times(\overline{\mathbf{u}}-\mathbf{u}_d) \tag{2.1}$$

where $\sigma\equiv\sigma_t(1+\sigma_t)^{-1}$ and $\sigma_t = O(1)$ is the turbulent Prandtl number. The implication of the new term in (2.1) was first studied in CD5 and more quantitatively in sec. 2f of C18 where it was shown that it *lowers* the amount of energy that mesoscales draw from the mean potential energy, which in turn implies that the isopycnal slopes are steeper than in the GM model, see Fig.4 of C18. This feature becomes relevant when studying for example the implications of the predicted increase of the wind stress that tends to steepen the isopycnal slopes (Gent, 2016). The first GM term in (2.1) becomes the full eddy induced velocity only at the steering level where $\overline{\mathbf{u}} = \mathbf{u}_d$ at about 2km depth when mesoscales co-move with the mean velocity. Since Fig. 3 of C18 shows that above 2km, $\overline{u}\text{-}u_d > 0$ while $\overline{v}\text{-}v_d < 0$, in the ACC where f<0, one has ($A=\kappa_M/\sigma|f|r_d^2$):

$$u^{+}= u_{GM} + A\left|\overline{v}\text{-}v_d\right|, \qquad v^{+}= v_{GM} + A\left|\overline{u}\text{-}u_d\right| \tag{2.2}$$

and thus, the new term in (2.1) enhances *the eddy term* $\mathbf{u}^+ \cdot \nabla H$ and thus subduction.

b) D-regime

To parameterize the D-regime, SR employed a heuristic *tapering function T(x,y,z)* whereby the stream function is considered an extension of the first of (1.2) in the form (1.3):

$$\boldsymbol{\Psi}_D = -\kappa_M T(x,y,z)\mathbf{s} \times \mathbf{e}_z \tag{2.3}$$

and the eddy induced velocities read as follows:

$$\mathbf{u}^+ = -\frac{\partial}{\partial z}[\kappa_M\ T(x,y,z)\mathbf{s}], \qquad w^+ = \nabla_H \cdot [\kappa_M\ T(x,y,z)\mathbf{s}] \tag{2.4}$$

Though in principle T(x,y,z) depends on x,y,z , thus far it has always been taken to be a function of z only, an assumption that has the following implication. Consider the second relation in (2.4):

$$w^+ = \kappa_M \mathbf{s} \cdot \nabla_H T(x,y,z) + T(x,y,z)\nabla_H \cdot \mathbf{s}\kappa_M \tag{2.5}$$

The assumption that T(x,y,z) depends only on z makes the first term on the right hand side of (2.5) vanish which affects the subduction rates. As for T(z), SR adopted a straight line with the conditions T(0)=0 to ensure that $w^+(0) = 0$, see relation (1.4) of C18. If the A-D interface is denoted by h, matching (2.3) with (1.2) requires that T(h)=1 but the choice of h is not trivial. For example, Gnanadesikan et al. (2007) concluded that a tapering approach yielded OGCMs results that were "disconcerting" because of the strong dependence of h on the isopycnal slope at that depth. Finally, while tapering functions may work as a numerical devise, the physical content of the D-regime can hardly be represented that way since, as discussed in sec.1b of C18, the A-D regimes satisfy very different conservation laws, i.e., potential vorticity in the A-regime with an inverse energy cascade and relative vorticity in the D-regime with enstrophy cascade.

To avoid tapering functions, one needs a parameterization of the D-regime which turned out to be a difficult task as shown by the seven different heuristic parameterizations that were proposed (cited in sec.1b of C18). Since no unique formulation emerged, Canuto and Dubovikov (2011, CD11) employed invariance properties and physical arguments and derived the following eddy stream function:

$$\boldsymbol{\Psi}^{+} = - \frac{F_v(\overline{b})}{N^2 \left|\mathbf{s}^2\right|} \mathbf{s} \times \mathbf{e}_z \tag{2.6}$$

which is valid in both A-D regimes, e.g., in the A-regime $F_v(\overline{b}) = \kappa_M N^2 \left|\mathbf{s}^2\right|$ yields (1.2). The vertical buoyancy flux $F_V(\overline{b})$ was given in Eq. (3.1)-(3.2) of C18 that we rewrite in a form as close as possible to the one in the A-regime:

$$F_V(\overline{b}) = \kappa_M N^2 \mathbf{s} \cdot \boldsymbol{\Sigma} \quad , \quad \boldsymbol{\Sigma} = \boldsymbol{\omega} \times \mathbf{e}_z , \quad fr_d^2 \boldsymbol{\omega} \quad \equiv z\mathbf{u}_D + \int_0^z \mathbf{u}_D(z')dz' \tag{2.7}$$

where $\mathbf{u}_D = \overline{\mathbf{u}} - \mathbf{u}_d$. It must be pointed out that using a mesoscale resolving numerical simulation, Luneva et al. (2015) presented a detailed assessment of the flux (2.7) under a variety of external forcing. Using (2.7) into (2.6), the latter acquires the form (2.3) with the tapering function now given by the following relation:

$$T(x,y,z) = \left|\mathbf{s}^2\right|^{-1} \mathbf{s} \cdot \boldsymbol{\Sigma} \tag{2.8}$$

which shows that T(x,y,z) is a function of x,y,z and that is no longer arbitrary but given by the mesoscale model itself. Fig. 7 of C18 shows that (2.8) yields results lower than the commonly used straight line.

c) Extent of the D-regime

Since the D-regime extent h is not determined by a mesoscale model, SR, their Eq.(4) and Salle'e and Rintoul (2010), their Eq.(11), assumed:

$$h=H \tag{2.9}$$

which is not in accordance with results of numerical simulations showing that below the mixed layer the flow is still diabatic (Mensa et al., 2013; Veneziani et al., 2014; Ramachandran et al., 2014). The inadequacy of (2.9) was also discussed by Gregory (2000, sec.2). The D-regime is characterized by strong vertical mixing due to wind stress that destabilizes the stable stratification represented by the positive square of the Brunt- Väisälä frequency. In the KPP vertical mixing schemes (Large et al., 1994), the strong mixing ceases at a depth where the *bulk Richardson number* becomes O(1). Such a depth is called the boundary layer depth HBL and is location dependent. While the choice of HBL as the *lower limit* of h is well motivated, it is still not sufficient since one also needs to know how deep h can be. In that respect, we suggest that h *should be less than the depth of the thermocline* since at that depth, the stratification would be too strong for the D-regime to exist. We thus suggest the following heuristic expression:

$$h = \frac{1}{2}[\mathrm{HBL} + \text{depth of max } N^2(z)] \tag{2.10}$$

Buckingham et al. (2017, sec.4.3.2) also suggested the existence of lower and upper bounds for h which they called $H_{1,2}$; the upper bound was the depth of peak stratification as in (2.10) but the lower bound was still taken to be the mixed layer depth rather than the HBL. In Fig.1 we plot the ratio h/H in the ACC, where h is computed using (2.10) and the mixed layer depth H is computed from the potential density criterion $\Delta\sigma = 0.03$kg m^{-3}. The results in Fig.1 show that in the majority of locations h>H or $h \approx H$ in accordance with previous authors (e.g., Mensa et al.,2013) and Veneziani et al. (2014) found h >H. At the same time, the results also show that it is possible that h<H in some locations, as suggested by an anonymous referee.

d) Mesoscale diffusivity

The mesoscale diffusivity κ_M is a key ingredient in any mesoscale parameterization and the difficulties in determining it are demonstrated by the variety of suggestions that were made, e.g., sec.3c of Salle'e et al. (2010). Thus far, all the suggested expressions were heuristic and one can surmise the following time sequence of models of increasing physical content:

$$\kappa_M(\text{constant}) \rightarrow \kappa_M(2D) \rightarrow \kappa_M \propto N^2 \rightarrow \kappa_M(3D) \tag{2.11}$$

The first entry is no longer viable since it leads to no-eddy saturation (Gent, 2016); the 2D model is an improvement but fails to reproduce WOCE (2002) data showing the vertical structure of the eddy kinetic energy with enhanced surface values, see Fig.1 of C19. To account for this feature, Salle'e et al. (2010) adopted the third relation in (2.11) in which N^2 was considered a proxy for the eddy kinetic energy. While an improvement, it does not provide the full x,y dependence shown by the T/P data (Scharffenberg and Stammer, 2010) which can only be obtained by constructing the last entry in (2.11), a model of the 3D $\kappa_M(x,y,z)$.

The strength and reliability of any $\kappa_M(x,y,z)$ model depends on how accurately the key ingredient, the eddy kinetic energy K(x,y,z), reproduces the WOCE (2002) data for the vertical profile and the T/P data (Scharffenberg and Stammer, 2010) for the x,y surface values. Canuto and Dubovikov (1996, Eq. 24) derived the expression for the turbulent viscosity felt by an eddy of size ℓ caused by all the eddies smaller than ℓ. Sec.2 of C19 discusses how that expression is applied to the present oceanic context and further shows how it contains the well-known mixing length theory as a particular case. The structure of the mesoscale diffusivity given by Eq.(2.5) of C19 is:

$$\kappa_M = \alpha r_d K^{1/2} \varpi(\mathbf{u}_D, K) \tag{2.12}$$

where $\alpha \cong ½$ represents the departure from the mixing length theory, as explained in relations (2.3)-(2.4) of C19; r_d is the Rossby deformation radius, K(x,y,z) is the 3D eddy kinetic energy and $\varpi(\mathbf{u}_D,\mathrm{K})$ represents the interaction of mesoscales with the mean velocity $\overline{\mathbf{u}}$. To use (2.12), one must parameterize the eddy kinetic energy K(x,y,z) and the barotropic mesoscale drift velocity:

$$\mathrm{K(x,y,z)} = \Gamma(\mathrm{z})\ \mathrm{K_s(x,y)}, \qquad \mathbf{u}_d(\mathrm{x,y}) \tag{2.13}$$

Bates et al. (2014) determined the variables in (2.13) using today's data with the resulting diffusivity shown in their Fig.10a. Since this procedure lacks predictive power, it may not be suited for climate studies when future increase in wind strength may significantly change the eddy kinetic energy from today's value. To parameterize the functions (2.13), we employ the eddy drift velocity given by Eq. (2.5) of C18 and its assessment vs. T/P data shown in Fig.1 of that paper. In CD5, the vertical structure of K was derived to be:

$$\Gamma(\mathrm{z}) = \left|1+\mathrm{a}_0\right|^{-2} \left|\mathrm{a}_0+\mathrm{B}_1(\mathrm{z})\right|^2 \tag{2.14}$$

where $\mathrm{B}_1(\mathrm{z})$ is the first baroclinic mode (Wunsch, 1997), $\mathrm{a}_0^2 = |\mathrm{B}_1(-\mathrm{H}_b)|$ represents the barotropic contribution and Fig.1 of C19 shows the comparison of (2.14) with WOCE (2002) data in different regions. The more difficult determination of $\mathrm{K_s(x,y)}$ was discussed in detail in sec.4 of C19 with the result given by Eq.(4.10) and the assessment against T/P data (Scharffenberg and Stammer, 2010) is shown in Fig. 9-10. It is relevant to point out that both vertical and horizontal components of K(x,y,z) were expressed analytically. Finally, the function $\varpi(\mathbf{u}_D,\mathrm{K})$ was derived to be:

$$\varpi(\mathbf{u}_D,\mathrm{K}) = \left(1+\frac{|\mathbf{u}_D|^2}{\mathrm{K}}\right)^{-1/2} \tag{2.15}$$

For small values of $|\mathbf{u}_D|^2 K^{-1}$, (2.15) recovers the heuristic expression used by Bates et al. (2014). Fig. 5 of C19 shows the comparison of (2.12) with NATRE data (North Atlantic Tracer Release Experiment, Ferrari and Polzin, 2005).

3. OGCM results from C18-C19 parameterizations

In addition to the tests discussed above, we used the new mesoscale parameterization in the GISS-ER stand-alone OGCM (see Appendix B) under CORE-I forcing (Griffies et al., 2009). The 500 year run yielded the results in Figs. 12-17 of C19 showing the global ocean temperature, the Atlantic overturning circulation, the meridional heat transport, the Drake Passage transport all of which were compared with the results of 17 previous OGCMs; finally, Fig. 18 of C19 shows how the model reproduces the winter ACC mixed layer depths.

4. Mesoscale diffusivity and subduction rates

The mesoscale diffusivities derived by Salle'e et al. (2008) using surface drifter data were larger than those used in the SR model and reproduced more closely the SOSE data. This motivated SR to suggest to boost the diffusivity in (1.2)-(1.4) tenfold. Since the subduction rates we obtain shown in Fig. 2 reproduce satisfactorily the SOSE data, it remains to be shown that the mesoscale diffusivities predicted by the present model reproduce the surface drifter data. Before we do so, we need to remark that the reason to study the case c) with $w^+ = 0.3$ was to highlight the contribution of w^+ since Hiraike et al. (2016), using an eddy resolving simulation, reported that the w^+ contribution is large; indeed, Fig.2c shows that with $w^+ = 0$, the resulting subduction rates do not reproduce the SOSE data. Next, consider Fig.3. The 3D diffusivities of this model shown in the left panel compare well with the results in Fig.3 of Salle'e et al. (2008); for completeness, the right panel shows the 2D diffusivities used by SR.

5. Conclusions

The two models for the mesoscale diffusivity Eq .(1.4) employed by SR yielded subduction rates smaller than SOSE data by an order of magnitude. On the other hand, the mesoscale diffusivities derived by Salle'e et al. (2008) from surface drifter data were lager than those in (1.4) and reproduced more closely the data. Thus, SR suggested to boost the diffusivity (1.4) tenfold. In this work, we used the mesoscale parameterizations presented in C18-C19 whose implications were assessed against a variety of data before being used in the subduction problem that represents an additional test of the C18-C19 parameterizations. Use of the latter reproduced satisfactorily topology (subduction equator-ward and obduction poleward) and magnitudes of the SOSE data. Finally, since it was previously shown (Canuto et al., 2018) that sub-mesoscales also produce sizeable subduction but with a topology different than that of mesoscales, a complete picture will require that mesoscales and sub-mesoscales are considered together.

Acknowledgements

VMC thanks Prof. Y. Tanaka and Prof. D.Marshall for informative correspondence. The authors thank two referees for questions that helped sharpen our presentation. Resources supporting this work were provided by the NASA High-End Computing (HEC) Program through the NASA Center for Climate Simulation (NCCS) at the Goddard Space Flight Center.

Appendix A

Mesoscale parameterization for coarse resolution OGCMs

The mesoscale parameterizations in C18-C19 is summarized as follows. The OGCMs solve the equations for the mean momentum and mean arbitrary tracers, the latter being both active tracers (such as T,S) and passive (such CO2) which have different parameterizations. In C18-C19 we treated the effect of mesoscales on an arbitrary tracer since the parameterization of the mesoscale-induced momentum fluxes (Reynolds stresses) are not yet available (work is in progress). Diabatic-D and adiabatic-A regimes are governed by different conservation laws and have different parameterizations.

General relations

Diabatic-D regime. The equation governing a mean tracer $\overline{\tau}$ reads as follows:

$$\partial_t \overline{\tau} + \overline{\mathbf{U}} \cdot \nabla \overline{\tau} + \nabla \cdot \mathbf{F}(\overline{\tau}) = \mathrm{Q} \qquad \text{(A1)}$$

where $\overline{\mathbf{U}} = (\overline{\mathbf{u}}, \overline{\mathrm{w}})$ is the 3D mean velocity, $\mathbf{F}(\overline{\tau}) = \mathbf{F}_{\mathrm{H}}(\overline{\tau}) + \mathbf{e}_z \mathrm{F}_{\mathrm{v}}(\overline{\tau})$ is the 3D mesoscale-induced tracer flux, $\mathbf{e}_z$ =(0,0,1) and Q represents external forcing. The *horizontal* flux is given by:

$$\mathbf{F}_{\mathrm{H}}(\overline{\tau}) = -\kappa_{\mathrm{M}} \cdot \nabla_{\mathrm{H}} \overline{\tau} \qquad \text{(A2)}$$

where κ_M is the mesoscale diffusivity discussed below . The *vertical tracer flux* is given by:

$$F_v(\bar{\tau}) = -\kappa_M \Phi \boldsymbol{\Omega}^{\parallel} \cdot (\nabla_H \bar{\tau} + \nabla_\rho \bar{\tau}) - \kappa_M (1\text{-}\Phi) \boldsymbol{\Omega} \cdot \nabla_H \bar{\tau}, \qquad \boldsymbol{\Omega}^{\parallel} = |\mathbf{s}|^{-2}\, \mathbf{s} \cdot \boldsymbol{\Omega} \mathbf{s} \tag{A3}$$

where:

$$\nabla_\rho \bar{\tau} = \nabla_H \bar{\tau} + \mathbf{s}\partial_z, \qquad \Phi(z) = \frac{z^2}{h_*^2}\frac{N^2}{N_*^2}, \qquad \Phi(0) = 0, \quad \Phi(-h_*) = 1 \tag{A4}$$

Here, N is the Brunt-Vaisala frequency, **s** is the slope of the isopycnals and h_* denotes the depth of the D-regime. The function $\Phi(z)$ allows to match the flux at h_* with that of the A-regime. We have:

Tracer: surface, $F_v(\bar{\tau})$ =0, bottom D-regime, $F_v(\bar{\tau}) = -\kappa_M \boldsymbol{\Omega}^{\parallel} \cdot (\nabla_H \bar{\tau} + \nabla_\rho \bar{\tau})$

(A5)

Buoyancy: surface, $F_v(\bar{b})$ =0, bottom D-regime, $F_v(\bar{b}) = -\kappa_M \boldsymbol{\Omega}^{\parallel} \cdot \nabla_H \bar{b} = \kappa_M N^2 \boldsymbol{\Omega} \cdot \mathbf{s}$

$$\boldsymbol{\Omega}(z) = [\boldsymbol{\omega}(z) \times \mathbf{e}_z - \Phi(z)\boldsymbol{\omega}_* \times \mathbf{e}_z] + \Phi(z)\frac{N(z)^2}{N_*^2}\mathbf{s}(z)$$

$$f r_d^2 \boldsymbol{\omega}(z) \equiv z\mathbf{u}_D - \int_z^0 \mathbf{u}_D(z')dz', \qquad \mathbf{u}_D = \bar{\mathbf{u}} - \mathbf{u}_d \tag{A6}$$

where and r_d is the first Rossby deformation radius. In the case of buoyancy:

Buoyancy: at $z = \text{-}h_*$, $\boldsymbol{\Omega} = \mathbf{s}$, $F_v(\bar{b}) = \kappa_M N^2 \left|\mathbf{s}^2\right|$ (A7)

The last relation coincides with the GM form of the vertical buoyancy flux given by the GM model.

Adiabatic-A regime. The thickness-weighted (isopycnal) averages used to express the equations in this regime does not coincide with the Eulerian averages appropriate to the D-regime. The different types of averages bring a new vector **E** in the mean racer equation that now reads as follows:

$$\partial_t \overline{\tau} + \overline{\mathbf{U}} \cdot \nabla \overline{\tau} + \nabla \cdot \mathbf{F}(\overline{\tau}) = Q \quad , \qquad \mathbf{F}(\overline{\tau}) = \mathbf{F}_{skew}(\overline{\tau}) + \mathbf{F}_{redi}(\overline{\tau}) + \mathbf{E}(\overline{\tau}) \tag{A8}$$

The skew flux is such that $\nabla \cdot \mathbf{F}_{skew} = \mathbf{U}^{+} \cdot \nabla \overline{\tau}$, where $\mathbf{U}^{+} = (\mathbf{u}^{+}, w^{+})$ is the non-divergent, 3D eddy induced velocity and the Redi flux is $\mathbf{F}_{redi} = -\kappa_M (\nabla_\rho \overline{\tau} + \mathbf{s} \cdot \nabla_\rho \overline{\tau}\, \mathbf{e}_z)$**.** Finally:

$$\mathbf{E} = -\frac{r_d^2}{K}\frac{\partial K}{\partial z}(\mathbf{e}_z \times \mathbf{u}_D \cdot \nabla_\rho \overline{\tau})\mathbf{e}_z \times \mathbf{s} \tag{A9}$$

where K is the eddy kinetic energy. Due to the smallness of this term, it will be neglected hereafter.

Eddy induced velocity:

$$\mathbf{u}^{+} = \mathbf{u}^{+}_{GM} - \frac{\kappa_M}{f r_d^2}\mathbf{e}_z \times \mathbf{c}_R + \frac{\kappa_M}{\sigma f r_d^2}\mathbf{e}_z \times (\overline{\mathbf{u}} - \mathbf{u}_d) \tag{A10}$$

In compact form:

$$\mathbf{u}^{+} = -\frac{\partial}{\partial z}\kappa_M \boldsymbol{\xi} \quad , \qquad \kappa_M(z)\boldsymbol{\xi}(z) = -\int_{-H_b}^{z} \mathbf{u}^{+}(z')dz' \qquad \text{(A11)}$$

where $\sigma \equiv \sigma_t(1+\sigma_t)^{-1}$, σ_t is the turbulent Prandtl number of O(1), $\mathbf{c}_R = r_d^2 \mathbf{e}_z \times \boldsymbol{\beta}$, $\boldsymbol{\beta} = \nabla f$ is the Rossby wave velocity and H_b is the ocean depth.

Drift velocity:

$$\mathbf{u}_d(x,y) = \sigma \mathbf{c}_R + <\bar{\mathbf{u}}> - \sigma f r_d^2 \mathbf{e}_z \times (<\frac{\partial \mathbf{s}}{\partial z}> - \frac{\mathbf{s}_*}{H_*}) \qquad \text{(A12)}$$

where the average <..> is defined as follows:

$$<\varphi> = \frac{\int_{-H_b}^{-h_*} \varphi(z)\kappa_M(z)dz}{\int_{-H_b}^{-h_*} \kappa_M(z)dz} \quad , \qquad H_* \equiv \frac{\int_{-H_b}^{-h_*} \kappa_M(z)dz}{\kappa_M(h_*)} \qquad \text{(A13)}$$

and in (A12), $\mathbf{s}_*$ is the isopycnal slope at h_*.

Mesoscale diffusivity κ_M

$$\kappa_M = \alpha r_d K^{1/2} \varpi(\mathbf{u}_D, K) , \qquad \varpi = [1 + \frac{1}{K}|\mathbf{u}_D|^2]^{-1/2} \qquad \text{(A14)}$$

where $\alpha \simeq 1/2$.

Eddy kinetic energy

$$K(x,y,z) = \Gamma(x,y,z)\, K_s(x,y) \qquad \text{(A15)}$$

where $\Gamma(x,y,z)$ is the vertical profile and $K_s(x,y)$ is the surface value. We have:

$$\Gamma(x,y,z) = \left|1+a_0\right|^{-2} \left|a_0+B_1(z)\right|^2, \qquad a_0 = \left|B_1(\text{-}H_b)\right|^{1/2} \qquad \text{(A16)}$$

Here, $B_1(z)$ is the first baroclinic mode solution of the eigenvalue problem $\partial_{zz}\varphi + (N/fr_d)^2\varphi = 0$, $\varphi = N^{-2}\partial_z B_1$ with the boundary conditions $\partial_z B_1 = 0$ at z = - H_b, 0 and $B_1(0)=1$. The surface kinetic energy K_s was derived to be given by:

$$K_s = \alpha_K^{-1}(1+BD)^{-1}(K_A + K_D) \quad , \quad BD \equiv [\int_{-H_b}^{0} \Gamma(z)dz]^{-1} \int_{-H_b}^{-h_*} \gamma(z)\Gamma(z)dz$$

$$\alpha_K \equiv (C_k r_d)^{-1} \int_{-H_b}^{0} \Gamma^{3/2}(z)dz, \qquad C_K \equiv (\frac{3}{2}Ko)^{3/2}\sigma_t^{1/2}, \qquad 4 \le Ko \le 8$$

$$K_A = \alpha r_d \int_{-H_b}^{-h_*} \varpi\Gamma^{1/2}(z)N^2\mathbf{s}\cdot\xi dz, \qquad K_D = \alpha r_d \int_{-h_*}^{0} \varpi\Gamma^{1/2}(z)N^2\mathbf{s}\cdot\mathbf{\Omega}dz$$

$$\gamma(z) = (2/\pi)^{1/2}(H_b/\delta_b)\exp(-\zeta^2/2), \qquad \zeta \equiv (z+H_b)\delta_b^{-1}, \qquad \delta_b = 40\text{m} \qquad \text{(A17)}$$

where Ko is the Kolmogorov constant.

Depth of the D-regime:

$$h_* = \frac{1}{2}[\mathrm{HBL} + \max N^2(z)] \qquad \text{(A18)}$$

where HBL, defined in Large et al. (1994, pages 371-372), is the depth at which the bulk Richardson number relative to the surface reaches values 0.3-1

Implementation in an OGCM

The 3D mesoscale induced tracer flux is written in the tensor form:

$$\mathbf{F}(\bar{\tau}) = -\kappa_M \mathbf{K} \cdot \nabla\bar{\tau} \qquad \text{(A19)}$$

where:

A-regime:

$$\mathbf{K} = \begin{pmatrix} 1 & 0 & s_x - \xi_x \\ 0 & 1 & s_y - \xi_y \\ s_x + \xi_x & s_y + \xi_y & s^2 \end{pmatrix} \qquad \text{(A20)}$$

D-regime:

$$\mathbf{K} = \begin{pmatrix} 1 & 0 & 0 \\ 0 & 1 & 0 \\ K_{31} & K_{32} & K_{33} \end{pmatrix} \qquad \text{(A21)}$$

$$K_{31} = (1\text{-}\Phi)\Omega_x + 2\Phi\Omega_x^{\parallel}, \qquad K_{32} = (1\text{-}\Phi)\Omega_y + 2\Phi\Omega_y^{\parallel}, \qquad K_{33} = \mathbf{\Omega} \cdot \mathbf{s} \tag{A22}$$

Appendix B. The OGCM

We employed the 3D diffusivity tensor for an arbitrary tracer given in sec.7 of C18, the mesoscale diffusivity (3.5) and the KPP vertical mixing scheme (Large et al., 1994) in the GISS ER-model which is the ocean component of the coupled NASA GISS model E (Russell et al., 1995; Russell et al., 2000; Liu et al., 2003). An early version of the revised E2-R code was run in a stand-alone mode (Danabasoglu et al., 2014). It employs a mass coordinate approximately proportional to pressure with 32 vertical layers with thickness from ≈12m near the surface to ≈ 200m at the bottom. The horizontal resolution is 1.25° (longitude) by 1° (latitude). It is a fully dynamic, non-Boussinesq, mass-conserving free-surface ocean model using a quadratic upstream scheme for the horizontal advection of tracers and a centered difference scheme in the vertical. A 1800s time step is used for tracer evolution. Sea-ice dynamics, thermodynamics and ocean–sea-ice coupling are represented as in the CMIP5 model-E configuration (Schmidt et al., 2014), save that here ice is on the ocean model grid. To force the model, we used the CORE-I Protocol (Griffies et al., 2009) with fluxes obtained from bulk formulae the inputs to which are the ocean model surface state and atmospheric conditions derived from a synthesis of observations that repeat the seasonal cycle of a “normal year”. The results we present correspond to the output of the final 20 winters (JAS) of a 500 year run.

References

Bates, M., R.Tulloch, J.Marshall and R.Ferrari, 2014, Rationalizing the spatial distribution of mesoscale eddy diffusivity in terms of mixing length theory, *J.Phys Oceanogr.,* **44**, 1523-1540, doi: 10.1175/JPO-D-13-0130.1

Buckingham, C. E., Z. Khaleel, A. Lazar, A. P. Martin, J. T. Allen, A. C. Naveira Garabato, A. F.Thompson, and C. Vic, 2017, Testing Munk's hypothesis for sub-mesoscale eddy generation using observations in the North Atlantic, *J. Geophys. Res. Oceans,* **122**, 6725–6745, doi:10.1002/2017JC012910

Canuto, V.M. and M.S.Dubovikov, 1996, A dynamical model for turbulence. General Formalism, *The Phys. of Fluids*, **8**, 571-586

Canuto, V.M. and M.S.Dubovikov, 2005, Modeling mesoscale eddies, *Ocean Model.* **8**, 1-30;

Canuto, V.M. and M.S. Dubovikov, 2011, Comparison of four mixed layer mesoscale parameterizations and the equations for an arbitrary tracer, *Ocean. Model*., **39,** 200-2007

Canuto, V.M, M.S.Dubovikov, Y.Cheng, A.M.Howard and A.Leboissetier, 2018, Parameterization of mixed layer and deep ocean mesoscales including non-linearity, *J.Phys.Oceanogr,***48**, 555-572, doi: 10.1175/JPO-D-16-0255, cited as C18

Canuto, V.M., Y. Cheng and A.M.Howard, 2018, Subduction by sub-mesoscales, *J. Geophys. Res: Oceans,* **123**, 8688-8700

Canuto, V.M., Y. Cheng, A.M.Howard and M.S.Dubovikov, 2019, Three dimensionally space dependent mesoscale diffusivity. Derivation and implications, *J.Phys.Oceanogr***., 49,** 1055-1074, doi: 10.1175/JPO-D-18-0123.1, cited as C19

Chelton, D.B., M.G.Schlax and R.M.Samelson, 2011, Global observations of non-linear mesoscale eddies, *Progress in Oceanography*, **91**, 167-216, cited as C11

Cushman-Roisin, 1987, Dynamics of the ocean surface mixed layer, Hawaii Inst of Geophysics Special Publication, P.Muller and D. Henderson, Eds.

Danabasoglu, G. and 45 co-authors, 2014: North Atlantic simulations in Coordinated Ocean-reference experiment phase II (CORE-II). Part I: Mean states, *Ocean Model.*, **73**, 76-107,doi:10.1016/j.ocemod.2013.10.00

Ferrari, R. and K.I.Polzin, 2005, Finescale structure of the T-S relation in the eastern North Atlantic, *J.Phys.Oceanogr.*, **35**, 1437-1454, doi:101175/JPO2763.1

Gent, P.R., and J.C. McWilliams, 1990, Isopycnal mixing in ocean circulation models, *J. Phys. Oceanogr.*, *20*, 150-155

Gent, P.R., 2016, Effects of Southern Hemisphere wind changes on the meridional overturning circulation, *Ann. Rev. Marine Science*, 8, 79-94

Gregory, J.M., 2000, Vertical heat transports in the ocean and their effect on time dependent climate change, *Climate Dynamics,* **16**, 501-515

Griffies and B.L. Samuels, 2007, Effects in a climate model of slope tapering in neutral physics schemes, *Ocean Model.*, **16**, 1-16

Griffies, S.M. and 23 co-authors, 2009, Coordinated Ocean-ice Reference Experiments (COREs), *Ocean Model.,* **26,** 1-46.

Hiraike, Y, Y.Tanaka and H.Hasumi, 2016, Subduction of Pacific Antarctic Intermediate Water in an eddy-resolving model, *J. Geophys. Res., Oceans*, **121**, 133-147, doi:10.1002/2015JC010802

Klocker, A. and D. Marshall, 2014, Advection of baroclinic eddies by depth mean flow, *Geophys. Res. Lett.*, **41**, 3517-3521

Large, W.G., J.C. McWilliams and S.C. Doney, 1994, Oceanic vertical mixing: A review and a model with a nonlocal boundary layer parameterization, *Rev. of Geophys.,* **32**, 363-403, doi.org/10.1029/94RG01872

Liu, J., G. A. Schmidt, D. G. Martinson, D. Rind, G. L. Russell and X. Yuan 2003, Sensitivity of sea ice to physical parameterizations in the GISS global climate model, *J. Geophys.es.* **108**, no. C2, 3053, doi:10.1029/2001JC001167

Luneva, M.V., C.A.Clayson, M.S.Dubovikov, 2015, Effects of mesoscale eddies in an active mixed layer: test of the parameterization in eddy resolving simulations *Geophys. &Astrophys. Fluid Dyn.,* doi:10.1080/03091929.2015.1041023

Marshall, D., 1997, Subduction of water masses in an eddying ocean, *J.Mar.Res,* **55**, 201-222

Mazloff, M.R., P. Heimbach and C. Wunsch, 2010, An eddy-permitting Southern Ocean State Estimate (SOSE), *J. Phys. Oceanogr*, **40**, 880-889

McWilliams, J.C., 1985, Sub-mesoscales, coherent vortices in the ocean, *Rev. Geophys*., 23,165182, doi:10.1029/RG023I002P00165

Mensa, J.A., Z.Garraffo, A.Griffa, T.M.Ozgokmen, A.Haza and M.Veneziani, 2013, Seasonality of sub-mesoscale dynamics in the Gulf Stream region, *Ocean Dynamics*, **63**, 21-43

Ramachandran, S. A.Tandon and A. Mahadevan, 2014, Enhancement in vertical fluxes at a front by mesoscale-submesoscale coupling, *J.Geophys. Res*., *Oceans*, doi: 10.1002/2014JC010211

Russell, G.L., J. R. Miller, D. H. Rind, 1995. A coupled atmosphere-ocean model for transient climate change, *Atmos. Ocean* **33,** 683-730

Russell, G.L., J. R. Miller, D. H. Rind, R. A. Ruedy, G. A. Schmidt and S. Sheth, 2000, Comparison of model and observed regional temperature changes during the past 40 +years, *J. Geophys. Res.* **105**, 14891-14898

Sallee', J.B., K. Speer, R. Morrow and R.Lumpkin, 2008, An estimate of Lagrangean eddy statistics and diffusion in the mixed layer of the Southern Ocean, *J.Marine Res*., **66**, (4), 441-463

Sallee', J.B., K. Speer, S. Rintoul and S. Wijffels, 2010, Southern Ocean thermocline ventilation, *J. Phys. Oceanogr*., **40,** 509-529

Sallee', J.B. and S.R.Rintoul, 2011, Parameterization of eddy-induced subduction in the Southern Ocean surface layer, *Ocean Model*., **39**, 146-153, SR11

Scharffenberg, M.G. and D.Stammer, 2010, Seasonal variations of the geostrophic flow field and of eddy kinetic energy inferred from Topex/Poseidon and Jason-1 Tandem Mission Data, *J.Geophys. Res*., 115, C2, doi 10.1029/2008JC005242

Schmidt, G.A. and 44 co-authors, 2014, Configuration and assessment of the GISS ModelE2 contributions to the CMIP5 archive. *J. Adv. Model. Earth Syst*., **6**, no. 1, 141-184, doi:10.1002/2013MS000265

Sloyan, B. and S. Rintoul, 2001, Circulation, renewal and modification of Antarctic Mode Water and Intermediate Water, *J. Phys. Oceanogr*., **31,** 1005-1030

Veneziani, M., A.Griffa, Z.Garrafo and J.A.Mensa, 2014, Barrier layers in the tropical South Atlantic: mean dynamics and sub-mesoscale effects, *J. Phys.Oceanogr*., **44**, 265-288

Visbeck, M., J. Marshall, T.Haine and M. Spall, 1997, Specification of eddy transfer coefficients in coarse resolution ocean circulation models. *J. Phys. Oceanogr*. **27**, 381-402

WOCE Data Products Committee, 2002, WOCE Global Data, Version 3.0, WOCE International Project Office, WOCE Report No. 180/02, Southampton, UK, cited as WOCE (2002)

Wunsch, C., 1997, The vertical partition of oceanic horizontal kinetic energy, *J. Phys.Oceanogr.,* **27**, 1770-1794

Figure caption

Fig. 1 ACC map of h Eq.(2.10) in units of the mixed layer depth H computed using the potential density criterion $\Delta\sigma = 0.03 \text{kg m}^{-3}$. The results correspond to an average of the last 20 year winters (JAS) of a 500 year OGCM run.

Fig. 2 a) subduction rates from SOSE (reproduced from SR), b) subduction rates from the present mesoscales model, c) subduction rates from the present model with $w^+ = 0$. The results correspond to an average of the last 20 year winters (JAS) of a 500 year OGCM run.

Fig.3 Left panel: surface $\kappa_M (m^2 s^{-1})$ from for 3D model; right panel, $\kappa_M (m^2 s^{-1})$ from 2D model. The results correspond to an average of the last 20 year winters (JAS) of a 500 year OGCM run.

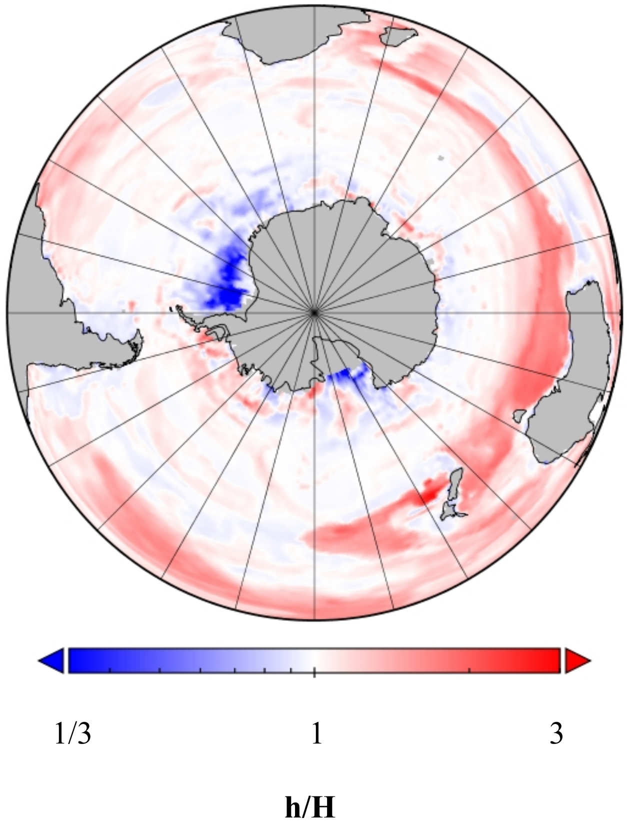

Fig. 1 ACC map of h Eq.(2.10) in units of the mixed layer depth H computed using the potential density criterion $\Delta\sigma = 0.03 kg\ m^{-3}$. The results correspond to an average of the last 20 year winters (JAS) of a 500 year OGCM run.

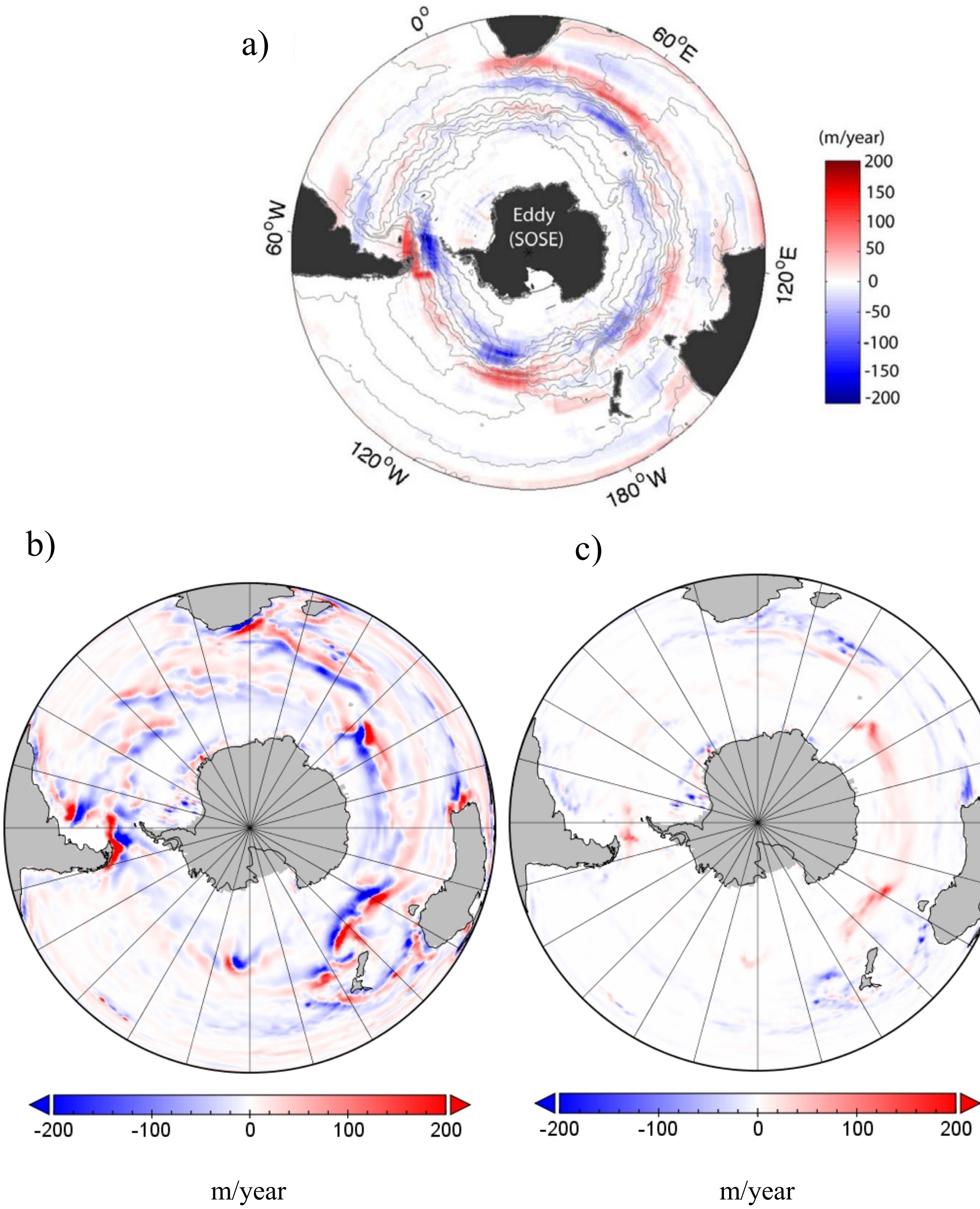

Fig. 2 a) subduction rates from SOSE (reproduced from SR), b) subduction rates from the present mesoscales model, c) subduction rates from the present model with $w^{+} = 0$. The results correspond to an average of the last 20 year winters (JAS) of a 500 year OGCM run.

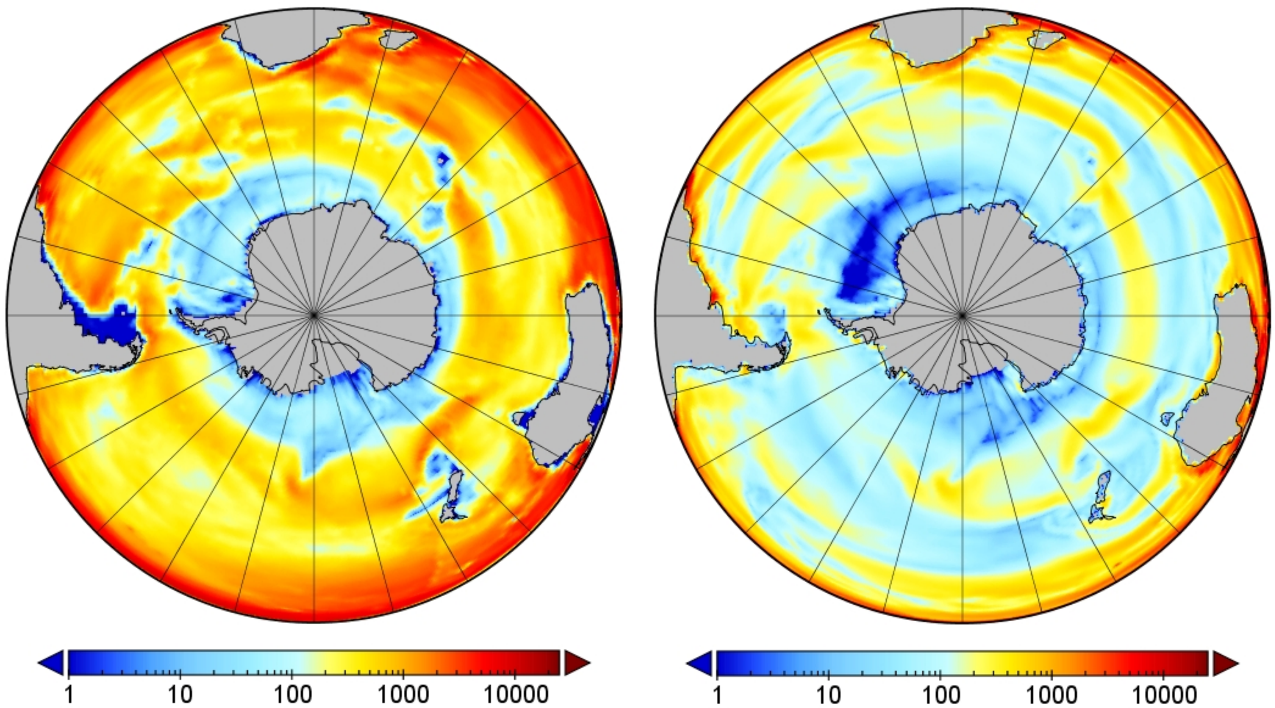

Fig.3 Left panel: surface $\kappa_M (m^2 s^{-1})$ from for 3D model; right panel, $\kappa_M (m^2 s^{-1})$ from 2D model. The results correspond to an average of the last 20 year winters (JAS) of a 500 year OGCM run.